Title

NMR and EPR-DEER Structure of a Dimeric Guanylate Cyclase Activator Protein-5 from Zebrafish Photoreceptors

Journal

Biochemistry, 60(41)

ISSN

0006-2960

Authors

Cudia, Diana
Roseman, Graham P
Assafa, Tufa E
et al.

Publication Date

2021-10-19

DOI

10.1021/acs.biochem.1c00612

Peer reviewed

HHS Public Access

Author manuscript

Biochemistry. Author manuscript; available in PMC 2022 March 24.

Published in final edited form as:

Biochemistry. 2021 October 19; 60(41): 3058–3070. doi:10.1021/acs.biochem.1c00612.

NMR and EPR-DEER Structure of a Dimeric Guanylate Cyclase Activator Protein-5 from Zebrafish Photoreceptors

Diana Cudia,
Department of Chemistry, University of California, Davis, California 95616, United States

Graham P. Roseman,
Department of Chemistry and Biochemistry, University of California, Santa Cruz, California 95064, United States

Tufa E. Assafa,
Department of Chemistry and Biochemistry, University of California, Santa Cruz, California 95064, United States

Manisha Kumari Shahu,
Division of Biochemistry, Department of Neuroscience, University of Oldenburg, 26129 Oldenburg, Germany

Alexander Scholten,
Division of Biochemistry, Department of Neuroscience, University of Oldenburg, 26129 Oldenburg, Germany

Sarah-Karina Menke-Sell,
Division of Biochemistry, Department of Neuroscience, University of Oldenburg, 26129 Oldenburg, Germany

Hiroaki Yamada,
Department of Chemistry, University of California, Davis, California 95616, United States

Karl-W. Koch,
Division of Biochemistry, Department of Neuroscience, University of Oldenburg, 26129 Oldenburg, Germany

Glenn Milhauser,

Corresponding Author: **James B. Ames** – *Department of Chemistry, University of California, Davis, California 95616, United States;* Phone: (530) 752-6358; jbames@ucdavis.edu.

Author Contributions

J.B.A. designed research and, with input from other authors, wrote the paper. D.C., G.P.R., T.E.A., M.K.S., A.S., S.-K.M.-S., H.Y., K.-W.K., G.M., and J.B.A. performed research. D.C., G.P.R., T.E.A., A.S., and J.B.A. analyzed data.

Supporting Information

The Supporting Information is available free of charge at https://pubs.acs.org/doi/10.1021/acs.biochem.1c00612.
HSQC NMR spectra of Mg^{2+}-free versus Mg^{2+}-bound GCAP5 (Figure S1), EPR-DEER data of all spin-labeled GCAP5 constructs and their corresponding distance distributions (Figure S2), HSQC NMR spectrum of $GCAP5^{H18A/Y21A}$ and MALS analysis of $GCAP5^{H18A/Y21A}$ and $GCAP5^{R22A}$ (Figure S3), and GCAP5 melting temperature analysis (Figure S4) (PDF)

Accession Codes

Atomic coordinates for GCAP5: PDB entry 7M2M.

Complete contact information is available at: https://pubs.acs.org/10.1021/acs.biochem.1c00612

The authors declare no competing financial interest.

Department of Chemistry and Biochemistry, University of California, Santa Cruz, California 95064, United States

James B. Ames
Department of Chemistry, University of California, Davis, California 95616, United States

Abstract

Retinal guanylate cyclases (RetGCs) are regulated by a family of guanylate cyclase-activating proteins (called GCAP1–7). GCAPs form dimers that bind to Ca^{2+} and confer Ca^{2+} sensitive activation of RetGC during visual phototransduction. The GCAP5 homologue from zebrafish contains two nonconserved cysteine residues (Cys15 and Cys17) that bind to ferrous ion, which stabilizes GCAP5 dimerization and diminishes its ability to activate RetGC. Here, we present NMR and EPR-DEER structural analysis of a GCAP5 dimer in the Mg^{2+}-bound, Ca^{2+}-free, Fe^{2+}-free activator state. The NMR-derived structure of GCAP5 is similar to the crystal structure of Ca^{2+}-bound GCAP1 (root-mean-square deviation of 2.4 Å), except that the N-terminal helix of GCAP5 is extended by two residues, which allows the sulfhydryl groups of Cys15 and Cys17 to become more solvent exposed in GCAP5 to facilitate Fe^{2+} binding. Nitroxide spin-label probes were covalently attached to particular cysteine residues engineered in GCAP5: C15, C17, T26C, C28, N56C, C69, C105, N139C, E152C, and S159C. The intermolecular distance of each spin-label probe in dimeric GCAP5 (measured by EPR-DEER) defined restraints for calculating the dimer structure by molecular docking. The GCAP5 dimer possesses intermolecular hydrophobic contacts involving the side chain atoms of H18, Y21, M25, F72, V76, and W93, as well as an intermolecular salt bridge between R22 and D71. The structural model of the GCAP5 dimer was validated by mutations (H18E/Y21E, H18A/Y21A, R22D, R22A, M25E, D71R, F72E, and V76E) at the dimer interface that disrupt dimerization of GCAP5 and affect the activation of RetGC. We propose that GCAP5 dimerization may play a role in the Fe^{2+}-dependent regulation of cyclase activity in zebrafish photoreceptors.

Graphical Abstract

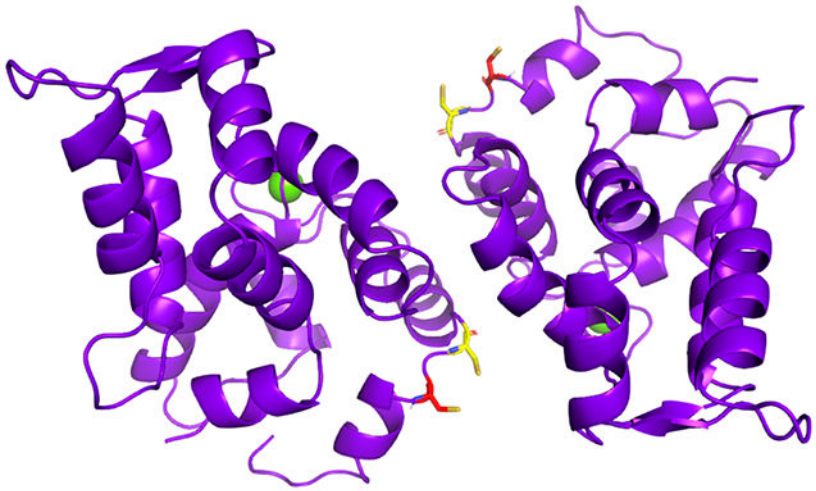

Retinal guanylate cyclase-activating proteins (GCAP1[1] and GCAP2[2]) are EF-hand calcium sensor proteins in mammalian photoreceptor rod and cone cells[3] that control Ca^{2+} sensitive activation of retinal guanylate cyclases (RetGCs[4,5]), which regulates the recovery phase of vertebrate visual phototransduction.[6,7] Ca^{2+} binds to the second, third, and fourth EF-hands in the GCAP proteins[8,9] (shaded red, cyan, and yellow, respectively, in Figure 1), and the Ca^{2+}-bound GCAPs bind to and inhibit RetGCs in dark-adapted photoreceptors.[10,11] By contrast, Mg^{2+} binds to the second EF-hand in GCAP1,[12] and the Ca^{2+}-free, Mg^{2+}-bound GCAPs activate RetGCs in light-adapted photoreceptors.[10,11] Mutations in both GCAP1 and RetGCs that disrupt the Ca^{2+}-dependent cyclase activation are genetically linked to retinal degenerative diseases.[13–17] GCAP orthologues are also expressed in zebrafish photoreceptors (GCAP3–5 and -7[18]). *In situ* hybridization showed that expression of zebrafish specific GCs and GCAPs coincides with the onset of visual function.[19,20] The zebrafish GCAP5 homologue has the most divergent amino acid sequence (Figure 1), which contains two nonconserved cysteine residues (Cys15 and Cys17) that were shown recently to ligate ferrous ion,[21] and the binding of Fe^{2+} to GCAP5 greatly diminishes its ability to activate RetGC.[21] Ferrous ion has been shown to serve as a redox sensor in a variety of cell types,[22] and it is tempting to speculate that redox sensing by GCAP5 might control phototransduction in zebrafish photoreceptors. Indeed, the accumulation of iron levels in the retina has been correlated with age-related macular degeneration in humans, suggesting the involvement of redox sensitive processes in the pathogenesis of the disease.[23]

In this study, we present NMR structures of Mg^{2+}-bound, Ca^{2+}-free, Fe^{2+}-free GCAP5 (hereafter termed Mg^{2+}-bound GCAP5), which represents the first structure of a GCAP protein in an activator state that binds to and activates RetGC. Overall, Mg^{2+}-bound GCAP5 is structurally similar to the crystal structure of Ca^{2+}-bound GCAP1[9] [2.4 Å root-mean-square deviation (RMSD)]. However, the N-terminal and C-terminal helices, located outside of the EF-hand motifs of GCAP5, are structurally distinct from those of Ca^{2+}-bound GCAP1, and the Ca^{2+}-induced structural changes to these helices may play a role in regulating RetGC and may facilitate binding of Fe^{2+} to GCAP5. We also present an EPR-DEER structural analysis to determine intermolecular contacts in the GCAP5 dimer. Nitroxide spin-label probes were introduced at 10 different sites in GCAP5 [C15, C17, T26C, C29, N56C, C69, C105, N139C, E152C, and S159C (see Figure 1)], and intermolecular distances from each site in the GCAP5 dimer were measured. The DEER distance restraints define a GCAP5 dimer structure that contains key hydrophobic residues (H18, Y21, M25, F72, V76, and W93) as well as an intermolecular salt bridge between R22 and D71 at the dimer interface.

MATERIALS AND METHODS

Cloning, Expression, and Purification of GCAP5.

Recombinant myristoylated GCAP5 (hereafter termed GCAP5) was used throughout this study, and bacterial expression of myristoylated GCAP5 was accomplished by coexpressing the GCAP5 D3N mutant[24] and yeast *N*-myristoyl CoA transferase (NMT) in *Escherichia coli* strain BL21(DE3) as described previously[24] for GCAP1.[12] Acylation of the GCAP5 D3N mutant was originally confirmed in living cells by a click-chemistry approach.[24]

Cloning of all mutants used in this study was similar to that described for other point mutants of GCAPs.[25,26] Purification of GCAP5 (and mutants) was achieved using previously described methods.[21] The GCAP5 variants used in guanylate cyclase assays were purified by employing a HiTrap Q HP column (5 mL, Cytiva) in the anion exchange chromatography step (application of a gradient from 0 to 1 M NaCl in 20 column volumes).

Analytical Size Exclusion Chromatography (SEC).

The molar mass of GCAP5 in the presence of Mg^{2+} (5 mM) was measured using analytical SEC (Superdex 200 HR 10/30 column, GE Healthcare) as described previously.[21] A sample volume of 100 μL of GCAP5 (200 μM protein concentration) was applied to the column equilibrated with 30 mM MES (pH 6.6), 5 mM citrate, and 100 mM NaCl. The SEC measurements were taken at 4 °C with a flow rate of 0.5 mL/min.

NMR Spectroscopy.

GCAP5 samples for NMR experiments consisted of ^{15}N-labeled or doubly ^{15}N- and ^{13}C-labeled myristoylated and Ca^{2+}-free, Mg^{2+}-bound GCAP5 (0.50 mM) dissolved in 30 mM MES (pH 6.5) buffer containing 2 mM DTT-d_{10}, 5 mM $MgCl_2$, and 93:7 H_2O/D_2O. All NMR experiments were performed at 30 °C on a Bruker 800 MHz Avance III spectrometer equipped with a triple resonance cryogenic TCI probe and pulsed field gradients. Two-dimensional ^{15}N–^{1}H HSQC and IPAP-HSQC experiments were performed with 2048 (^{1}H) × 256 (^{15}N) data points using ^{15}N-labeled GCAP5. Three-dimensional NMR HSQC-NOESY and HCCH-TOCSY experiments were performed and analyzed as described previously.[12] Spectra were processed using NMRPipe software package[27] and analyzed using SPARKY.[28]

Residual dipolar couplings (RDCs[29]) of GCAP5 were determined as described previously.[30] Briefly, the filamentous bacteriophage Pf1 (Asla Biotech Ltd., Riga, Latvia) was used as an orienting medium. Pf1 (12 mg/mL) was added to ^{15}N-labeled GCAP5 (0.5 mM) to produce weak alignment. ^{1}H–^{15}N residual dipolar coupling constants (D_{NH}) were measured using a 2D IPAP (inphase/antiphase) ^{1}H–^{15}N HSQC.[31] The backbone N–H RDCs were calculated by measuring the difference in ^{15}N splitting for each amide resonance in the presence and absence of the orienting medium. The RDC Q-factor and analysis of RDC data were calculated by PALES.[32]

NMR Structure Calculation.

NMR-derived structures of GCAP5 were calculated using restrained molecular dynamics simulations within Xplor-NIH.[33] Residual dipolar couplings, NOE distances, dihedral angles from TALOS+,[34] and backbone hydrogen bonds were used as structural restraints. NOEs were obtained via ^{15}N-edited NOESY-HSQC and ^{13}C-edited NOESY-HSQC experiments. Backbone dihedral angles were calculated by TALOS+ using backbone chemical shifts (Hα, Cα, Cβ, CO, ^{15}N, and HN) as input. The Xplor-NIH structure calculation was performed as described previously for GCAP1.[12] From a total of 200 structures, the 10 lowest-energy structures were deposited in the RCSB Protein Data Bank (PDB entry 7M2M). The structure quality was assessed by PROCHECK-NMR[35] and MolProbity.[36]

Spin Labeling and DEER Sample Preparation.

Protein samples were dialyzed against 4 L of dialysis buffer in 20 mM Tris (pH 7.4) with 100 μM TCEP overnight at 4 °C and diluted to 10–20 μM. The (1-oxyl 2,2,5,5-tetramethylΔ3-pyrroline-3-methyl) methanethiosulfonate spin-label (MTSSL, Toronto Research Chemicals Inc., Toronto, ON) was dissolved in dimethyl sulfoxide (DMSO) to a concentration of 40 mM. Excess MTSSL was added to the protein at a 30:1 molar ratio and then reacted on ice for 30 min. Unreacted spin-labels were removed by dialyzing overnight at 4 °C against 4 L of dialysis buffer containing 20 mM Tris (pH 7.4), which was repeated twice for >24 h. The protein was concentrated to a final concentration of ~300 μM by ultrafiltration using an Amicon spin concentrator. The final protein sample for DEER experiments was exchanged three times with 10 mM Tris-d_{11} (pH 7.4), 2 mM $MgCl_2$, and 99.9% D_2O. Before the sample was frozen, 25% glycerol-d_8 was added to the protein as a cryoprotectant.

EPR-DEER Measurements.

Four-pulse DEER data were collected on a Bruker ELEXSYS E580 spectrometer, capable of operation at both X-band and Q-band frequencies, equipped with an AWG bridge and a Q-band QT2 resonator. The pump pulse was fixed to the center peak in the field-swept nitroxide spectrum, and the probe frequency was set to be 100 MHz from this frequency. $\pi/2$ and π pulses were all 34 ns Gaussian pulses.[37] The delay between the first and second probe pulses was 400 ns, and dipolar evolution data were collected out to 1.5–8.0 μs. Experiments were performed at 50 K and were signal averaged for 4–16 h. The raw data were background-corrected and analyzed by Tikhonov regularization using DEERAnalysis.[38] CW-EPR spectra of the DEER samples were recorded at room temperature with a Bruker E500 CW-EPR spectrometer operating at the X-band frequency (~9.4 GHz) using an ER 4122SHQE resonator (Bruker).

Molecular Docking Calculation.

The web-based docking program HADDOCK[39] was used to generate a structural model of Mg^{2+}-bound GCAP5. The NMR structure of Mg^{2+}-bound GCAP5 was docked with itself to satisfy the intermolecular distance restraints measured by DEER. The docking calculation was initiated with a rigid body energy minimization that generated 1000 structures. The best 200 structures were subjected to a semiflexible simulated annealing step. In the final step, the 200 structures obtained from the previous simulated annealing step were refined in explicit waters. At the end of the HADDOCK dimer calculation, 10 structures formed a single cluster out of 200 water-refined structures. The coordinate file with the lowest HADDOCK score was chosen for the final structural model displayed in this study.

Guanylate Cyclase Assays.

To test the regulatory properties of wild type GCAP5 and it variants (mutants without C defined as 5A, H18A/Y21A, H18E/Y21E, R22A, R22D, M25E, N56C, N139C, and S159C), we reconstituted purified GCAP5 forms with cell membranes containing heterologously expressed human GC-E (orthologue of bovine and mice RetGC1) in HEK flip 293 cells essentially as described previously,[40,41] but using a cell line that stably expressed GC-E.

Cells were cultivated and harvested by centrifugation (300*g* for 5 min); the supernatant was discarded, and the pellet was resuspended in 100 μL of 50 mM HEPES-KOH (pH 7.4), 50 mM KCl, 20 mM NaCl, 1 mM DTT, and mammalian protease inhibitor cocktail (1:500). Cells were placed on ice for 20 min, disrupted by being passed several times through a syringe, and placed on ice again. Activities were measured according to a detailed protocol that was published previously[26,40] with the following modifications: GCAP5 was added at a final concentration of 3 μM, and GC activities were obtained by adjusting the free Ca^{2+} concentration using a K_2H_2EGTA/CaH_2EGTA buffer system as described previously.[26] The free Mg^{2+} concentration was 1 mM.

Light Scattering Experiments.

The molar mass of GCAP5 and mutants was assessed by using a multiangle light scattering (MALS) miniDawn instrument with a 690 nm laser (Wyatt Technologies, Inc.) coupled to a refractive index instrument (Optilab Rex, Wyatt Technologies, Inc.). The molar mass of chromatographed protein was calculated from the observed light scattering intensity and differential refractive index using ASTRA software (Wyatt Technologies, Inc.) based on a Zimm plot analysis using a refractive index increment ($dn/dc = 0.185$ L g^{-1}).[42,43]

RESULTS

NMR-Derived Structures of Mg^{2+}-Bound GCAP5.

NMR chemical shift assignments published previously for Mg^{2+}-bound GCAP5[44] were used in this study to determine NOESY-based distances, NMR-derived dihedral angle restraints, and residual dipolar coupling (RDC) restraints (Figure 2) that served as input for restrained molecular dynamics structure calculations (see Materials and Methods). The residual dipolar coupling magnitude and rhombicity were calculated by fitting the measured residual dipolar couplings to the calculated structure using the PALES program.[32] The RDC-refined structures have a quality *Q*-factor of 0.27 and an *R*-factor of 0.985 (Figure 2C). The NMR-derived structure of Mg^{2+}-bound GCAP5 (PDB entry 7M2M) was validated with PROCHECK: 90% of residues belonged to the most favorable region in the Ramachandran plot.

The NMR structures of Mg^{2+}-bound GCAP5 have a backbone RMSD of 1.0 Å (overlaid in Figure 3A), and structural statistics are listed in Table 1. The GCAP5 main chain structure (Figure 3B) contains a total of 11 α-helices and four β-strands: α1 (residues 8–15), α2 (19–27), α3 (35–41), α4 (50–62), α5 (72–82), α6 (88–97), α7 (108–121), α8 (130–140), α9 (151–160), α10 (162–172), α11 (175–182), β1 (32–34), β2 (69–71), β3 (105–107), and β4 (148–150). The secondary structure of the final NMR structure of Mg^{2+}-bound GCAP5 (Figure 3B) is slightly different from the secondary structure inferred from the chemical shift index.[44] In particular, the C-terminal helix (α11) defined by NOESY and RDC data was predicted to be a random coil based on chemical shift analysis.[44] The secondary structure elements of GCAP5 combine to form two separate domains: The N-terminal domain is formed by the N-terminal helix (α1), EF1 (green, residues 19–41), and EF2 (red, residues 50–82), and the C-terminal domain is formed by EF3 (cyan, residues 88–121), EF4 (yellow, residues 130–160), and C-terminal helices (α10 and α11 in Figure 3B). The

N-terminal helix (α1) of GCAP5 is extended by two residues compared to that of GCAP1 (Figure 1). This extension of α1 in GCAP5 causes the sulfhydryl side chains of Cys15 and Cys17 to become more solvent exposed compared to what they are in GCAP1, which may facilitate the binding of Fe^{2+} to GCAP5 (Figure 3C). The helix immediately adjacent to EF4 (α10, colored purple in Figure 3C) is one turn longer in Mg^{2+}-bound GCAP5 than in Ca^{2+}-bound GCAP1. Thus, α10 in GCAP5 is structurally identical to the Ca^{2+} switch helix reported for Ca^{2+}-free GCAP1.[12] The C-terminal helix (α11) is one-half turn shorter in Mg^{2+}-bound GCAP5 than in Ca^{2+}-bound GCAP1 (Figure 1). The Ca^{2+}-dependent structural differences in both α10 and α11 are consistent with a Ca^{2+}-myristoyl tug mechanism[45] seen previously for GCAP1.[12]

The NMR structure of GCAP5 contains Mg^{2+} bound at EF2 (orange sphere in Figure 3) as evidenced by characteristic Mg^{2+}-dependent amide chemical shift changes assigned to Gly68 in EF2.[44] Also, Mg^{2+}-induced NMR spectral changes for GCAP5 (Figure S1) further demonstrate binding of Mg^{2+} to GCAP5. The geometry of chelating amino acid residues in GCAP5 and the bound Mg^{2+} was not observed directly in our NMR study. Instead, the stereochemical geometry and chelation of Mg^{2+} bound at EF2 were modeled with structural constraints derived from the X-ray crystal structure of Mg^{2+}-bound CaM,[46] which closely resembles the Mg^{2+} binding site geometry conserved in other EF-hand proteins such as CaBP1[47] and CaBP4.[48] GCAP5 residues at positions 1, 3, and 5 of the EF-hand loop in EF2 were selected to chelate the bound Mg^{2+} (see D63, D65, and D67 in Figure 3A). Mutation of the corresponding residues in GCAP1 significantly weakens Mg^{2+} binding and prevents cyclase activation.[10] The four EF-hands of GCAP5 with one Mg^{2+} bound at EF2 (and no metal bound at EF1, EF3, or EF4) each adopt interhelical angles that are similar to those observed in the crystal structure of Ca^{2+}-bound GCAP1. The overall main chain structure of Mg^{2+}-bound GCAP5 is somewhat similar to that of the Ca^{2+}-bound GCAP1 crystal structure [RMSD = 2.4 Å (Figure 3D)]. For the Mg^{2+}-bound GCAP5 structure, the interhelical angles are 131° (EF1), 114° (EF2), 104° (EF3), and 107° (EF4). Thus, the three functional EF-hands in GCAP5 (EF2–EF4) each adopt a preformed open conformation in the Ca^{2+}-free state akin to that of calbindin D_{9k}[49] and other Ca^{2+} buffer proteins,[50] which may explain the very high nanomolar Ca^{2+} binding affinity for GCAP proteins.[51]

Intermolecular Distances of the GCAP5 Dimer Determined by EPR-DEER.

Previous studies demonstrated that GCAP5 forms a dimer in solution.[21] In the current study, we used EPR-DEER to measure intermolecular distances that were used as restraints to calculate a structural model of the GCAP5 dimer. The DEER data for GCAP5 (Figure 4) were analyzed to determine intermolecular distances between individual nitroxide spin-labels covalently attached to particular Cys residues on the protein surface (C15, C17, T26C, C28, N56C, C69, C105, N139C, E152C, and S159C). Wild type GCAP5 contains five native Cys residues (C15, C17, C28, C69, and C105), and single-Cys mutants were generated in each case by replacing the other four Cys residues with Ala. In addition, we introduced a non-native Cys at particular residues (T26C, N56C, N139C, E152C, and S159C) in a Cys-less background mutant of GCAP5 ($GCAP5^{CL}$) in which all five native Cys residues were replaced with Ala. A total of 10 single Cys mutants of GCAP5 were constructed for EPR-DEER: $GCAP5^{CL}$(A15C), $GCAP5^{CL}$(A17C), $GCAP5^{CL}$(T26C), $GCAP5^{CL}$(A28C),

GCAP5^{CL}(N56C), GCAP5^{CL}(A69C), GCAP5^{CL}(A105C), GCAP5^{CL}(N139C), GCAP5^{CL}(E152C), and GCAP5^{CL}(S159C).

Representative EPR-DEER data for GCAP5 with a nitroxide spin-label attached individually to each single-Cys mutant [G C A P 5$^{C L}$ (A 2 8 C), G C A P 5$^{C L}$ (N 5 6 C), and GCAP5^{CL}(A69C)] are shown in Figure 4 (Figure S2 shows DEER data for all 10 mutants). The DEER data in each case were modeled by a distance distribution with most probable intermolecular distances of 16 ± 4, 52 ± 5, and 43 ± 5 Å for GCAP1^{CL}(A28C), GCAP5^{CL}(N56C), and GCAP5^{CL}(A69C), respectively (Figure 4). The intermolecular DEER distances for all single Cys mutants of GCAP5 are listed in Table 2 and Figure S2.

Structural Model of a GCAP5 Dimer.

The intermolecular DEER distances for each spin-label attached to GCAP5 (Figure 5A and Table 2) were used as distance restraints within HADDOCK[52] to calculate the structure of the GCAP5 dimer as described in Materials and Methods. The measured DEER distances (Table 2) for the most part agree within experimental error with the calculated intermolecular distances in the GCAP5 dimer model (Figure 5A). The apparent deviation between the calculated versus observed distances for C15 and C17 (important for Fe^{2+} binding[21]) might reflect the dynamic disorder for these residues in the absence of Fe^{2+}. Much smaller distance deviations were observed for N56C, C69, N139C, and E152C because these residues are located in regions of regular secondary structure that are more rigidly held in place. The structure of the GCAP5 dimer (Figure 5A) contains intermolecular contacts between mostly hydrophobic residues (H18, Y21, M25, F72, V76, and W93) at the dimer interface. The closest contacts are formed between the hydrophobic side chain atoms of H18, M25, F72, V76, and W93 (colored red in Figure 5A). The intermolecular contacts with V76 are consistent with the previous observation that a V77E mutation abolished dimerization of GCAP1.[12] The aromatic side chain atoms of H18, Y21 (not shown), F72, and W93 make intermolecular contacts with each other at the dimer interface (Figure 5B). The GCAP5 dimer is also stabilized by an intermolecular salt bridge between the side chain atoms of R22 and D71 (Figure 5C). The GCAP5 dimer (Figure 5A) is structurally similar to the dimeric structural model reported recently for GCAP1.[53]

Mutant Lacking All Five Cys and DEER Mutants of GCAP5 Are Functionally Intact.

To verify whether the GCAP5 5A mutant (lacking all five Cys residues) and single-Cys mutants (N56C, N139C, and S159C) used in the DEER experiments are functionally intact, we measured the retinal guanylate cyclase activity in the presence of wild type GCAP5 and each mutant (Figure 6) in the presence and absence of Ca^{2+}. The data set includes two positive controls and one negative control. Incubation of cyclase activity with WT GCAP5 showed the activating property of GCAP5 and reproduced previous observations that WT GCAP5 lacks the Ca^{2+} dependence, which is typical for other GCAP isoforms.[21] The second positive control was the activity profile obtained with the 5A mutant that showed a canonical Ca^{2+} dependence of GC activation in which the cyclase activity at low Ca^{2+} activity levels was similar to that of WT GCAP5 but much lower at high Ca^{2+} concentrations. These results agree with our previous data showing that the presence of

Cys at positions 15 and 17 seems to interfere with the Ca^{2+} switch.[21] The negative control was the GC activity without addition of a GCAP variant (control in Figure 6), resulting in >10-fold lower basal GC activities. Activities of all other mutants were above the control level, showing that they were functionally intact. The guanylate cyclase activities in the presence of the Cys-less GCAP5 mutant (5A in Figure 6) and each of the DEER mutants (N56C, N139C, and S159C) are each qualitatively similar to that of wild type GCAP5 at low Ca^{2+} concentrations, demonstrating that these mutants are each capable of activating the cyclase and appear to be functionally intact. Furthermore, when the negatively charged amino acid in the H/Y-E and R22D mutants was replaced with Ala, activities increased, in the case of R22A to >5-fold higher than that of WT and 5A. Surprisingly, although the Ca^{2+} switch is operational in R22A, the Ca^{2+}-bound R22A activates the cyclase to a higher degree than the Ca^{2+}-bound wild type GCAP5 (see GC activation at high Ca^{2+} concentrations).

Mutations at the GCAP5 Dimer Interface.

The key amino acids that form intermolecular contacts at the GCAP5 interface (H18, Y21, R22, M25, D71, F72, V76, and W93) were mutated to form the following mutants: H18A/Y21A, H18E/Y21E, R22A, R22D, M25E, D71A, D71R, F72A, F72E, V76A, V76E, and W93E. The corresponding residues in GCAP1 are conserved (Figure 1), and the same mutations in GCAP1 (Y22E, M26E, F73E, V77E, and W94E) were shown previously to both weaken dimerization and abolish activation of the cyclase,[53] consistent with the idea that GCAP1 dimerization is necessary for cyclase activation. A similar result was seen for GCAP5. The GCAP5 dimerization site mutants (H18A/Y21A, H18E/Y21E, R22D, and M25E) each exhibited a >4-fold reduction in the level of activation of cyclase activity compared to that of the wild type (Figure 6). The GCAP5 dimerization site mutants (D71A, D71R, F72A, F72E, V76A, V76E, and W93E) were each expressed in the insoluble fraction of the bacterial lysate (called inclusion bodies), which prevented their characterization. The low solubility here suggests that these mutations may destabilize dimerization of GCAP5 that in turn could cause protein unfolding, which may explain the precipitation of the mutated proteins. A double mutant (H18E/Y21E and H81A/Y21A) and single mutants (R22A, R22D, and M25E) are somewhat more soluble, although a detectable fraction of each mutant could also be detected in inclusion bodies, in contrast to wild type GCAP5 that is not detected in inclusion bodies. The most soluble mutant (M25E) exhibited an NMR HSQC spectrum that was overall similar to that of the wild type (Figure 7A). However, a number of resonances assigned to residues near the dimer interface (H18, Y21, D71, and W93) and resonances near the center of the spectrum appear much broader in the M25E spectrum (Figure 7A, red). The observed peak broadening for the M25E mutant could be caused by chemical exchange broadening mechanisms associated with lower-affinity dimerization for M25E compared to wild type. The double mutants (H18E/Y21E and H18A/Y21A) each exhibited a highly heterogeneous NMR spectrum (Figure 7B for H18E/Y21E and Figure S3A for H18A/Y21A) in which at least four different amide peaks were assigned to G68 (circled in Figure 7B). This heterogeneity suggests a complex mixture of perhaps monomer, dimer, and higher-order oligomers, as evidenced by many broadened resonances in the center of the spectrum. A fraction of the H18E/Y21E mixture was isolated as a monomeric species (see chromatography elution profiles in panels C and D of Figure 7) with a molar mass of 24 ± 2 kDa determined by SEC-MALS for H18E/Y21E (Figure 7E)

and for H18A/Y21A (Figure S3B), in contrast to wild type GCAP5 that is mostly a dimer under the same conditions.[21] A similar monomeric fraction was isolated for R22D (see chromatography profiles in panels F and G of Figure 7) with a molar mass of 29 ± 4 kDa determined by SEC-MALS (Figures 7H). The same molar mass was determined for R22A (Figure S3C). Thus, the R22A, R22D, M25E, H18A/Y21A, and H18E/Y21E mutations each appear to weaken the dimerization of GCAP5 as predicted by the structure.

The protein folding melting temperature (T_m) was measured for the soluble GCAP5 dimerization site mutants (H18E/Y21E, R22D, and M25E) to probe the effect of these mutations on the protein folding stability (Figure S4). The T_m values of wild type GCAP5 and mutant proteins were determined by measuring NMR HSQC spectra at different temperatures. The NMR intensity of the downfield-shifted amide resonance assigned to Gly68 (characteristic of the folded protein, called I_{Gly68}) was monitored as a function of temperature. For wild type GCAP5, I_{Gly68} began to decrease as the temperature was increased above 47 °C and a T_m value (temperature at which I_{Gly68} decreased by 2-fold) was estimated to be 52 ± 1 °C. The T_m values for the H18E/Y21E, R22D, and M25E mutants were measured to be 48 ± 1, 49 ± 1, and 49 ± 1 °C, respectively. The lower T_m values for the dimerization site mutants compared to that of the wild type suggest that the intermolecular contacts at the dimer interface contribute to the overall protein folding stability.

DISCUSSION

In this study, we present the NMR structure of Mg^{2+}-bound GCAP5 (Figure 3) and EPR-DEER analysis (Figure 4) of the dimeric GCAP5 structure (Figure 5). The NMR structure of the Mg^{2+}-bound activator form of GCAP5 looks similar to that of the crystal structure of GCAP1 (Figure 3D, and RMSD = 2.4 Å).[9] However, an important structural difference is that the N-terminal helix in GCAP5 is elongated by two residues, which allows the nonconserved sulfhydryl side chain of Cys15 and Cys17 to both point outward and chelate Fe^{2+} that can bind to GCAP5 (Figure 3C). The solvent-exposed side chains of Cys15 and Cys17 are consistent with previous studies that report high-affinity binding of Fe^{2+} to GCAP5.[21] The 10th helix (α10) of GCAP5 (colored purple in Figure 3) is elongated by three residues compared to the corresponding helix in Ca^{2+}-bound GCAP1 (Figure 1). The Ca^{2+}-induced shortening of α10 may explain how binding of Ca^{2+} to EF4 (directly connected to α10) is allosterically transmitted to the N-terminal myristoyl group and surrounding residues in GCAP1 (Y22, R23, M26, F73, and V77) that are responsible for activating guanylate cyclase.[54] This is consistent with the Ca^{2+}-myristoyl tug model[12,45] in which the binding of Ca^{2+} to the fourth EF-hand of GCAP1 (EF4) causes Ca^{2+}-induced conformational changes that “tug” on the downstream C-terminal helix that contacts the N-terminal myristoyl group, which alter the exposure of residues that are believed to interact with RetGC. Binding of Mg^{2+} to GCAP1 does not initiate the tug mechanism, because Mg^{2+} binds only to the second EF-hand and does not bind to EF4. The Ca^{2+}-myristoyl tug mechanism explains how GCAP1 activates guanylate cyclase and appears to operate in GCAP5, as well.

The structure of the GCAP5 dimer (Figure 5) was determined by docking two molecules of the NMR structure of GCAP5 (Figure 3) according to intermolecular distance restraints

determined by EPR-DEER (Figure 4 and Table 2). The GCAP5 dimer structure looks somewhat similar to the structure of the GCAP1 dimer (RMSD = 2.4 Å).[53] The dimer interface in both GCAP1 and GCAP5 consists of the same exposed hydrophobic residues (H18, Y21, M25, F72, V76, and W93) colored red in Figure 5A. Mutations at the GCAP5 dimerization site (H18E/Y21E, H18A/Y21A, R22D, and M25E) disrupt dimerization of GCAP5 (Figure 7) and decrease the level of cyclase activation by >4-fold (Figure 6). Interestingly, the point mutation p.H19Y in human GCAP1 that is located in the dimer interface was identified in patients diagnosed with retinitis pigmentosa. Investigation of the molecular properties of the H19Y GCAP1 mutant protein revealed a disruption of Ca^{2+} binding, guanylate cyclase regulation, and dimer formation,[55] which points to the importance of a dynamic monomer–dimer equilibrium for the function of human GCAP1, as well.[56] However, the exposed hydrophobic residues at the GCAP5 dimerization site have also been suggested to mediate contacts with RetGC.[54] It is possible that the exposed dimerization site in GCAP5 might prefer to interact with RetGC rather than promote GCAP5 dimerization in the presence of a saturating level of RetGC. This scenario is consistent with the R22A mutant, which causes a 5-fold increase in the level of cyclase activation (Figure 6) even though GCAP5 dimerization is weakened by R22A (Figure S3C). Future studies are needed to determine whether the GCAP5 dimer structure will remain intact upon binding to RetGC and how it might stabilize the transition state of the cyclase reaction.

An important structural difference between GCAP1 and GCAP5 is that the GCAP5 dimer is stabilized by an intermolecular salt bridge between R22 and D71 (Figure 5C) that is not seen in the GCAP1 dimer structure, perhaps because R22 in GCAP5 is replaced with a lysine in GCAP1 (Figure 1). Slight differences in the quaternary structures of dimeric GCAP1 and GCAP5 may explain the 3 Å increase in the intermolecular distance between K22 and D71 in GCAP1[53] compared to the much shorter salt bridge distance in GCAP5 (Figure 5C). We suggest that this difference in quaternary structure for GCAP1 and GCAP5 might explain why GCAP1 is 3-fold more potent at activating guanylate cyclase.[21]

The structure of the Ca^{2+}-free, Fe^{2+}-free, Mg^{2+}-bound GCAP5 dimer (Figure 5) is quite different from a structural model of the Fe^{2+}-bound GCAP5 dimer proposed previously.[21] In the Fe^{2+}-bound GCAP5 dimer, a single Fe^{2+} is chelated by the sulfhydryl side chains of Cys15 and Cys17 from each subunit of the GCAP5 dimer so that the intermolecular distance of the sulfhydryl atoms for Cys15 is <8 Å (see the double arrow in Figure 8). By stark contrast, in the Fe^{2+}-free GCAP5 dimer, the intermolecular distance of the nitroxide spin-label attached to Cys15 is 24 Å. The much larger intermolecular distance for Cys15 in the Fe^{2+}-free GCAP5 dimer (Figure 5 and Table 2) suggests that binding of Fe^{2+} to the GCAP5 dimer may cause the two protein subunits within the dimer to rotate with respect to one another as illustrated in Figure 8. This Fe^{2+}-induced rotation of the two protein subunits in the GCAP5 dimer dramatically alters the exposure of residues (H18, Y21, M25, F73, V76, and W93 highlighted by red ovals in Figure 8) that have been implicated in binding to guanylate cyclase.[54,55] We propose that the Fe^{2+}-dependent exposure of the cyclase binding site residues may explain how binding of Fe^{2+} to GCAP5 prevents its activation of guanylate cyclase. Future studies are needed to determine the atomic resolution structures of Fe^{2+}-bound GCAP5 and GCAP5 bound to guanylate cyclase to further test our model.

Supplementary Material

Refer to Web version on PubMed Central for supplementary material.

ACKNOWLEDGMENTS

The authors thank Jeff Walton and Ping Yu for help with NMR experiments.

Funding

This work was supported by National Institutes of Health (NIH) Grant R01-EY012347 to J.B.A., NIH Grants R35-GM131781 and S10-OD024980 to G.M., and Deutsche Forschungsgemeinschaft Grants KO948/15-1 and GRK1885 to K.-W.K. and to the Research Training Group in Oldenburg.

ABBREVIATIONS

DEER	double electron electron resonance
HSQC	heteronuclear single quantum coherence
MALS	multiangle light scattering
NMR	nuclear magnetic resonance
NOESY	NOE spectroscopy
RetGC	retinal guanylate cyclase
SEC	size exclusion chromatography

REFERENCES

(1). Palczewski K; Subbaraya I; Gorczyca WA; Helekar BS; Ruiz CC; Ohguro H; Huang J; Zhao X; Crabb JW; Johnson RS; et al. Molecular cloning and characterization of retinal photoreceptor guanylyl cyclase-activating protein. Neuron 1994, 13, 395–404. [PubMed: 7520254]

(2). Dizhoor AM; Olshevskaya EV; Henzel WJ; Wong SC; Stults JT; Ankoudinova I; Hurley JB Cloning, sequencing and expression of a 24-kDa Ca^{2+}-binding protein activating photoreceptor guanylyl cyclase. J. Biol. Chem 1995, 270, 25200–25206. [PubMed: 7559656]

(3). Palczewski K; Polans AS; Baehr W; Ames JB Ca(2+)-binding proteins in the retina: structure, function, and the etiology of human visual diseases. BioEssays 2000, 22, 337–350. [PubMed: 10723031]

(4). Dizhoor AM; Lowe DG; Olsevskaya EV; Laura RP; Hurley JB The human photoreceptor membrane guanylyl cyclase, RetGC, is present in outer segments and is regulated by calcium and a soluble activator. Neuron 1994, 12, 1345–1352. [PubMed: 7912093]

(5). Lowe DG; Dizhoor AM; Liu K; Gu Q; Spencer M; Laura R; Lu L; Hurley JB Cloning and expression of a second photoreceptor-specific membrane retina guanylyl cyclase (RetGC), RetGC-2. Proc. Natl. Acad. Sci. U. S. A 1995, 92, 5535–5539. [PubMed: 7777544]

(6). Koch KW; Duda T; Sharma RK Photoreceptor specific guanylate cyclases in vertebrate phototransduction. Mol. Cell. Biochem 2002, 230, 97–106. [PubMed: 11952100]

(7). Koch KW; Stryer L Highly cooperative feedback control of retinal rod guanylate cyclase by calcium ions. Nature 1988, 334, 64–66. [PubMed: 2455233]

(8). Ames JB; Dizhoor AM; Ikura M; Palczewski K; Stryer L Three-dimensional structure of guanylyl cyclase activating protein-2, a calcium-sensitive modulator of photoreceptor guanylyl cyclases. J. Biol. Chem 1999, 274, 19329–19337. [PubMed: 10383444]

(9). Stephen R; Bereta G; Golczak M; Palczewski K; Sousa MC Stabilizing function for myristoyl group revealed by the crystal structure of a neuronal calcium sensor, guanylate cyclase-activating protein 1. Structure 2007, 15, 1392–1402. [PubMed: 17997965]

(10). Peshenko IV; Dizhoor AM Ca2+ and Mg2+ binding properties of GCAP-1. Evidence that Mg2+-bound form is the physiological activator of photoreceptor guanylyl cyclase. J. Biol. Chem 2006, 281, 23830–23841. [PubMed: 16793776]

(11). Peshenko IV; Dizhoor AM Activation and inhibition of photoreceptor guanylyl cyclase by guanylyl cyclase activating protein 1 (GCAP-1): the functional role of Mg2+/Ca2+ exchange in EF-hand domains. J. Biol. Chem 2007, 282, 21645–21652. [PubMed: 17545152]

(12). Lim S; Peshenko IV; Olshevskaya EV; Dizhoor AM; Ames JB Structure of Guanylyl Cyclase Activator Protein 1 (GCAP1) Mutant V77E in a Ca2+-free/Mg2+-bound Activator State. J. Biol. Chem 2016, 291, 4429–4441. [PubMed: 26703466]

(13). Behnen P; Dell' Orco D; Koch KW Involvement of the calcium sensor GCAP1 in hereditary cone dystrophies. Biol. Chem 2010, 391, 631–637. [PubMed: 20370318]

(14). Dell'Orco D; Behnen P; Linse S; Koch KW Calcium binding, structural stability and guanylate cyclase activation in GCAP1 variants associated with human cone dystrophy. Cell. Mol. Life Sci 2010, 67, 973–984. [PubMed: 20213926]

(15). Payne AM; Downes SM; Bessant DA; Taylor R; Holder GE; Warren MJ; Bird AC; Bhattacharya SS A mutation in guanylate cyclase activator 1A (GUCA1A) in an autosomal dominant cone dystrophy pedigree mapping to a new locus on chromosome 6p21.1. Hum. Mol. Genet 1998, 7, 273–277. [PubMed: 9425234]

(16). Sokal I; Li N; Surgucheva I; Warren MJ; Payne AM; Bhattacharya SS; Baehr W; Palczewski K GCAP1 (Y99C) mutant is constitutively active in autosomal dominant cone dystrophy. Mol. Cell 1998, 2, 129–133. [PubMed: 9702199]

(17). Wilkie SE; Li Y; Deery EC; Newbold RJ; Garibaldi D; Bateman JB; Zhang H; Lin W; Zack DJ; Bhattacharya SS; Warren MJ; Hunt DM; Zhang K Identification and functional consequences of a new mutation (E155G) in the gene for GCAP1 that causes autosomal dominant cone dystrophy. Am. J. Hum. Genet 2001, 69, 471–480. [PubMed: 11484154]

(18). Imanishi Y; Yang L; Sokal I; Filipek S; Palczewski K; Baehr W Diversity of guanylate cyclase-activating proteins (GCAPs) in teleost fish: characterization of three novel GCAPs (GCAP4, GCAP5, GCAP7) from zebrafish (Danio rerio) and prediction of eight GCAPs (GCAP1–8) in pufferfish (Fugu rubripes). J. Mol. Evol 2004, 59, 204–217. [PubMed: 15486694]

(19). Fries R; Scholten A; Saftel W; Koch KW Zebrafish guanylate cyclase type 3 signaling in cone photoreceptors. PLoS One 2013, 8, e69656. [PubMed: 23940527]

(20). Ratscho N; Scholten A; Koch KW Expression profiles of three novel sensory guanylate cyclases and guanylate cyclase-activating proteins in the zebrafish retina. Biochim. Biophys. Acta, Mol. Cell Res 2009, 1793, 1110–1114.

(21). Lim S; Scholten A; Manchala G; Cudia D; Zlomke-Sell SK; Koch KW; Ames JB Structural Characterization of Ferrous Ion Binding to Retinal Guanylate Cyclase Activator Protein 5 from Zebrafish Photoreceptors. Biochemistry 2017, 56, 6652–6661. [PubMed: 29172459]

(22). Crack JC; Green J; Thomson AJ; Le Brun NE Iron-sulfur clusters as biological sensors: the chemistry of reactions with molecular oxygen and nitric oxide. Acc. Chem. Res 2014, 47, 3196–3205. [PubMed: 25262769]

(23). Sterling J; Guttha S; Song Y; Song D; Hadziahmetovic M; Dunaief JL Iron importers Zip8 and Zip14 are expressed in retina and regulated by retinal iron levels. Exp. Eye Res 2017, 155, 15–23. [PubMed: 28057442]

(24). Sulmann S; Vocke F; Scholten A; Koch KW Retina specific GCAPs in zebrafish acquire functional selectivity in Ca2+-sensing by myristoylation and Mg^{2+}-binding. Sci. Rep 2015, 5, 11228. [PubMed: 26061947]

(25). Fries R; Scholten A; Saftel W; Koch KW Operation profile of zebrafish guanylate cyclase-activating protein 3. J. Neurochem 2012, 121, 54–65. [PubMed: 22212098]

(26). Scholten A; Koch KW Differential calcium signaling by cone specific guanylate cyclase-activating proteins from the zebrafish retina. PLoS One 2011, 6, e23117. [PubMed: 21829700]

(27). Delaglio F; Grzesiek S; Vuister GW; Zhu G; Pfeifer J; Bax A NMRPipe: a multidimensional spectral processing system based on UNIX pipes. J. Biomol. NMR 1995, 6, 277–293. [PubMed: 8520220]

(28). Lee W; Tonelli M; Markley JL NMRFAM-SPARKY: enhanced software for biomolecular NMR spectroscopy. Bioinformatics 2015, 31, 1325–1327. [PubMed: 25505092]

(29). Tjandra N; Bax A Direct measurement of disances and angles in biomolecules by NMR in a dilute liquid crystalline medium. Science 1997, 278, 1111–1114. [PubMed: 9353189]

(30). Peshenko IV; Yu Q; Lim S; Cudia D; Dizhoor AM; Ames JB Retinal degeneration 3 (RD3) protein, a retinal guanylyl cyclase regulator, forms a monomeric and elongated four-helix bundle. J. Biol. Chem 2019, 294, 2318–2328. [PubMed: 30559291]

(31). Ottiger M; Delaglio F; Marquardt JL; Tjandra N; Bax A Measurement of dipolar couplings for methylene and methyl sites in weakly oriented macromolecules and their use in structure determination. J. Magn. Reson 1998, 134, 365–369. [PubMed: 9761712]

(32). Zweckstetter M NMR: prediction of molecular alignment from structure using the PALES software. Nat. Protoc 2008, 3, 679–690. [PubMed: 18388951]

(33). Schwieters CD; Kuszewski JJ; Tjandra N; Clore GM The Xplor-NIH NMR molecular structure determination package. J. Magn. Reson 2003, 160, 65–73. [PubMed: 12565051]

(34). Shen Y; Delaglio F; Cornilescu G; Bax A TALOS+: a hybrid method for predicting protein backbone torsion angles from NMR chemical shifts. J. Biomol. NMR 2009, 44, 213–223. [PubMed: 19548092]

(35). Laskowski RA; Rullmann JA; MacArthur MW; Kaptein R; Thornton JM AQUA and PROCHECK-NMR: programs for checking the quality of protein structures solved by NMR. J. Biomol. NMR 1996, 8, 477–486. [PubMed: 9008363]

(36). Chen VB; Arendall WB 3rd; Headd JJ; Keedy DA; Immormino RM; Kapral GJ; Murray LW; Richardson JS; Richardson DC MolProbity: all-atom structure validation for macromolecular crystallography. Acta Crystallogr., Sect. D: Biol. Crystallogr 2010, 66, 12–21. [PubMed: 20057044]

(37). Teucher M; Bordignon E Improved signal fidelity in 4-pulse DEER with Gaussian pulses. J. Magn. Reson 2018, 296, 103–111. [PubMed: 30241017]

(38). Jeschke G; Chechik V; Ionita P; Godt A; Zimmermann H; Banham J; Timmel CR; Hilger D; Jung H DeerAnalysis2006-a comprehensive software package for analyzing pulsed ELDOR data. Appl. Magn. Reson 2006, 30, 473–498.

(39). van Zundert GC; Rodrigues JP; Trellet M; Schmitz C; Kastritis PL; Karaca E; Melquiond AS; van Dijk M; de Vries SJ; Bonvin AM The HADDOCK2.2 Web Server: User-Friendly Integrative Modeling of Biomolecular Complexes. J. Mol. Biol 2016, 428, 720–725. [PubMed: 26410586]

(40). Koch KW; Helten A Guanylate cyclase-based signaling in photoreceptors and retina. In Signal Transduction in the Retina; Taylor and Francis, CRC Press: Boca Raton, FL, 2008; pp 121–143.

(41). Zagel P; Dell'Orco D; Koch KW The dimerization domain in outer segment guanylate cyclase is a Ca(2)(+)-sensitive control switch module. Biochemistry 2013, 52, 5065–5074. [PubMed: 23815670]

(42). Meyer M; Morgenstern B Characterization of gelatine and acid soluble collagen by size exclusion chromatography coupled with multi angle light scattering (SEC-MALS). Biomacromolecules 2003, 4, 1727–1732. [PubMed: 14606902]

(43). Wyatt PJ Combined differential light scattering with various liquid chromatography separation techniques. Biochem. Soc. Trans 1991, 19, 485. [PubMed: 1889645]

(44). Cudia D; Ames J Chemical shift assignments of retinal guanylyl cyclase activating protein 5 (GCAP5). Biomol. NMR Assignments 2019, 13, 201–205.

(45). Peshenko IV; Olshevskaya EV; Lim S; Ames JB; Dizhoor AM Calcium-myristoyl Tug. J. Biol. Chem 2012, 287, 13972–13984. [PubMed: 22383530]

(46). Senguen FT; Grabarek Z X-ray structures of magnesium and manganese complexes with the N-terminal domain of calmodulin: insights into the mechanism and specificity of metal ion binding to an EF-hand. Biochemistry 2012, 51, 6182–6194. [PubMed: 22803592]

(47). Li C; Chan J; Haeseleer F; Mikoshiba K; Palczewski K; Ikura M; Ames JB Structural insights into Ca2+-dependent regulation of inositol 1,4,5-trisphosphate receptors by CaBP1. J. Biol. Chem 2009, 284, 2472–2481. [PubMed: 19008222]

(48). Park S; Li C; Haeseleer F; Palczewski K; Ames JB Structural Insights into Activation of the Retinal L-type Ca2+ Channel (Cav1.4) by Ca2+-binding Protein 4 (CaBP4). J. Biol. Chem 2014, 289, 31262–31273. [PubMed: 25258313]

(49). Skelton NJ; Kordel J; Chazin WJ Determination of the solution structure of Apo calbindin D9k by NMR spectroscopy. J. Mol. Biol 1995, 249, 441–462. [PubMed: 7783203]

(50). Ikura M Calcium binding and conformational response in EF-hand proteins. Trends Biochem. Sci 1996, 21, 14–17. [PubMed: 8848832]

(51). Lim S; Peshenko IV; Dizhoor AM; Ames JB Effects of Ca2+, Mg2+, and myristoylation on guanylyl cyclase activating protein 1 structure and stability. Biochemistry 2009, 48, 850–862. [PubMed: 19143494]

(52). de Vries SJ; van Dijk M; Bonvin AM The HADDOCK web server for data-driven biomolecular docking. Nat. Protoc 2010, 5, 883–897. [PubMed: 20431534]

(53). Lim S; Roseman G; Peshenko I; Manchala G; Cudia D; Dizhoor A; Millhauser G; Ames J Retinal Guanylyl Cyclase Activating Protein 1 Forms a Functional Dimer. PLoS One 2018, 13, e0193947. [PubMed: 29513743]

(54). Peshenko IV; Olshevskaya EV; Lim S; Ames JB; Dizhoor AM Identification of target binding site in photoreceptor guanylyl cyclase-activating protein 1 (GCAP1). J. Biol. Chem 2014, 289, 10140–10154. [PubMed: 24567338]

(55). Abbas S; Marino V; Weisschuh N; Kieninger S; Solaki M; Dell'Orco D; Koch KW Neuronal Calcium Sensor GCAP1 Encoded by GUCA1A Exhibits Heterogeneous Functional Properties in Two Cases of Retinitis Pigmentosa. ACS Chem. Neurosci 2020, 11, 1458–1470. [PubMed: 32298085]

(56). Boni F; Marino V; Bidoia C; Mastrangelo E; Barbiroli A; Dell'Orco D; Milani M Modulation of Guanylate Cyclase Activating Protein 1 (GCAP1) Dimeric Assembly by Ca(2+) or Mg(2+): Hints to Understand Protein Activity. Biomolecules 2020, 10, 1408.

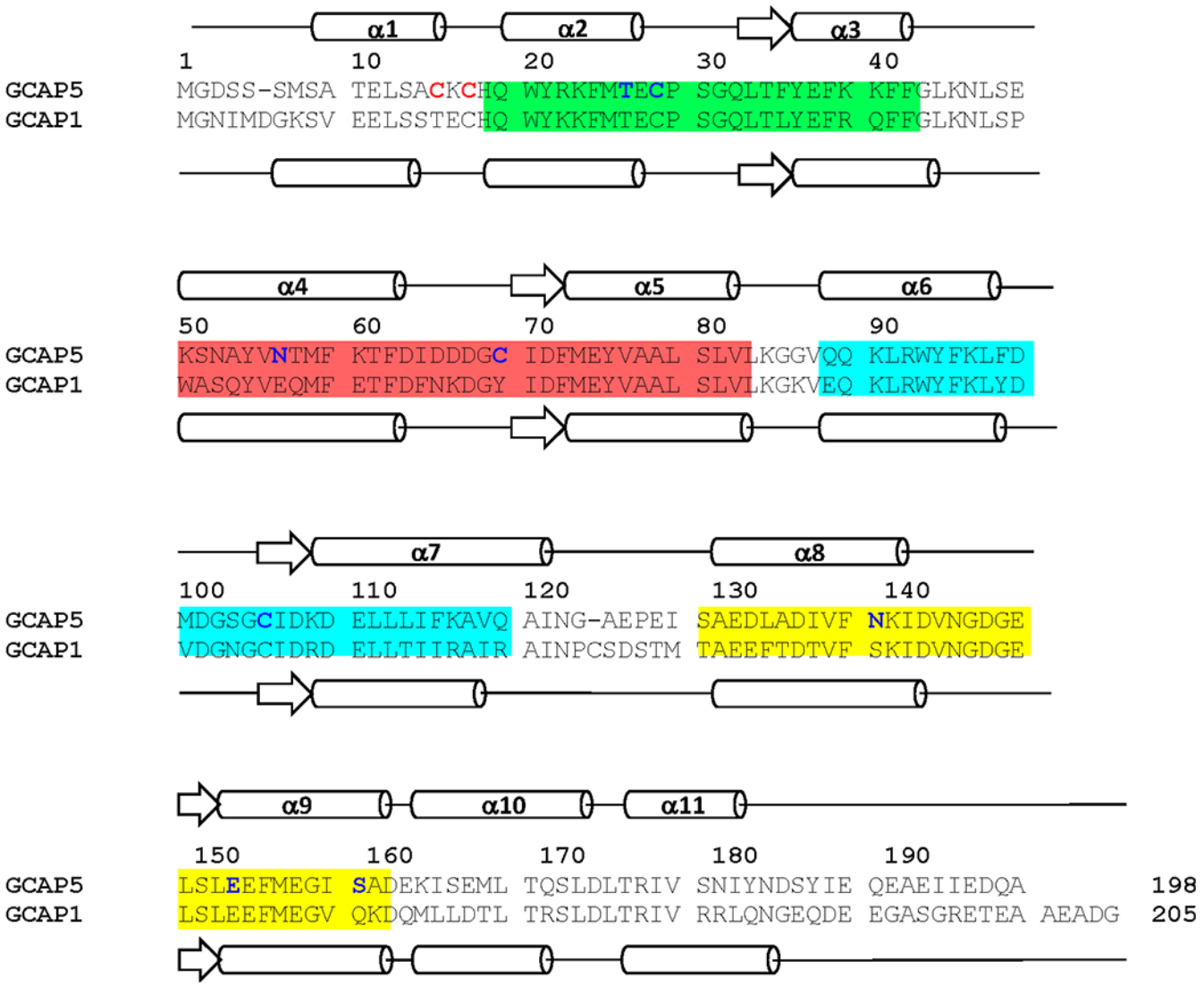

Figure 1.

Amino acid sequence alignment and secondary structure of GCAP1 and GCAP5. EF-hand motifs are shaded in color (green for EF1, red for EF2, cyan for EF3, and yellow for EF4). Nonconserved cysteine residues (C15 and C17) in GCAP5 are highlighted in red. Single cysteine residues (C15, C17, T26C, C28, N56C, C69, C105, N139C, E152C, and S158C) modified by nitroxide for DEER studies are highlighted in blue. α-Helices and β-strands are depicted by cylinders and arrows, respectively. Swiss Protein Database accession numbers are Q90WX4 (bovine GCAP1) and Q5MAC8 (zebrafish GCAP5).

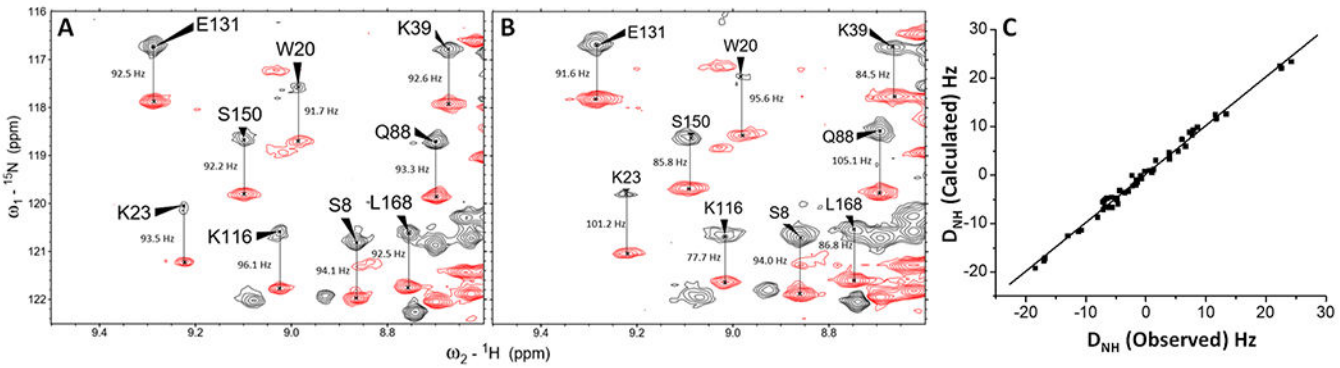

Figure 2.

Residual dipolar coupling (RDC) structural analysis of GCAP5. $^{1}H–^{15}N$ IPAP-HSQC spectra of Mg^{2+}-bound GCAP5 in the (A) absence and (B) presence of 12 mg/mL Pf1 phage. Observed spectral splittings in the absence of Pf1 (J_{NH}) and presence of Pf1 (J_{NH} + D_{NH}) are marked by vertical lines, and their difference was used to calculate RDCs as described in Materials and Methods. (C) RDCs calculated from the structure of Mg^{2+}-bound GCAP5 in Figure 3 plotted vs the RDCs measured in panel B show good agreement (Q-factor = 0.27, and R-factor = 0.985[32]).

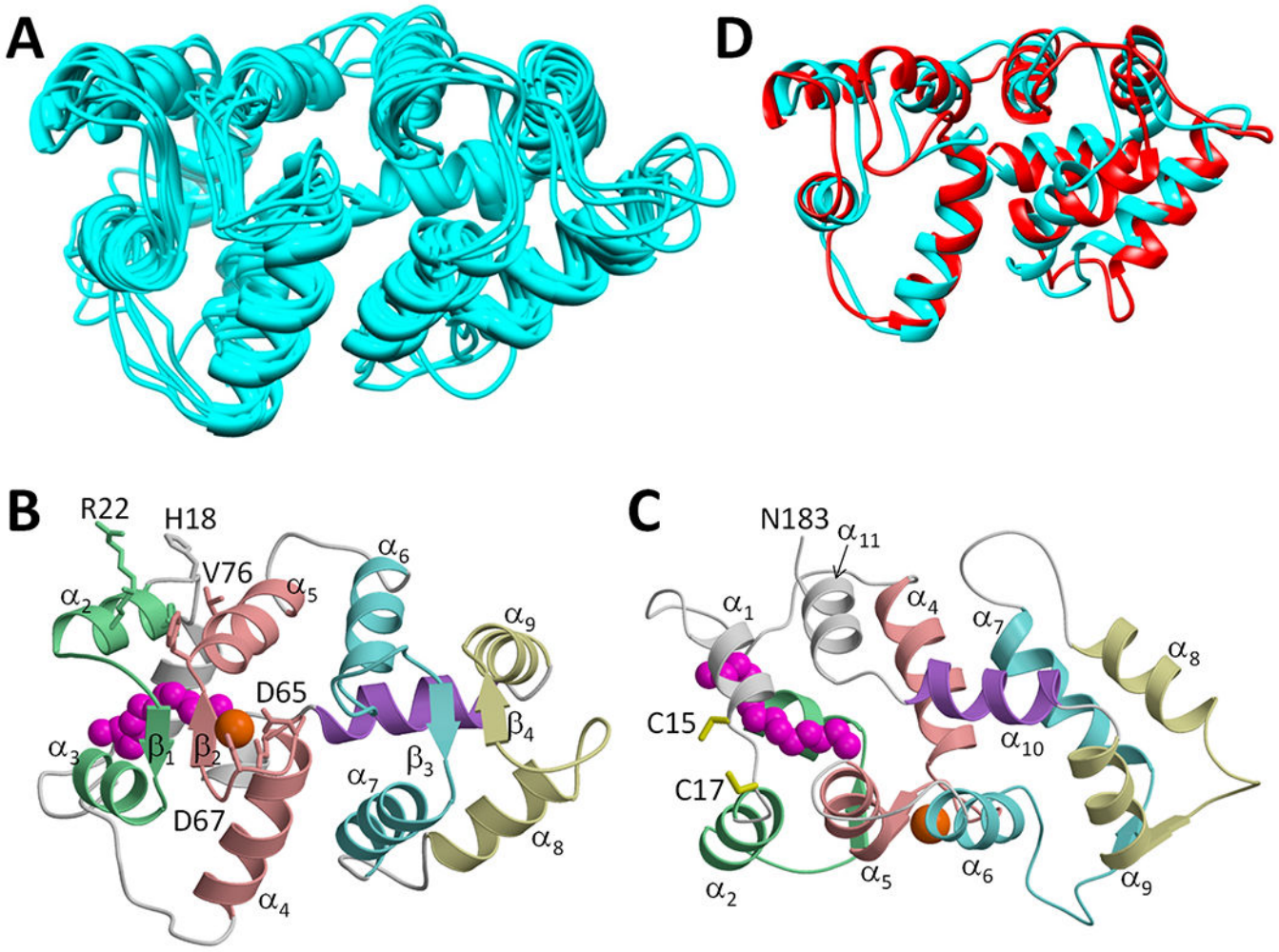

Figure 3.

NMR-derived structures of Mg^{2+}-bound GCAP5 (PDB entry 7M2M). (A) Ensemble of the 10 lowest-energy NMR structures. Structural statistics are listed in Table 1. (B) Average main chain structure of GCAP5 and (C) the same view rotated by 180° showing four EF-hands (colored as in Figure 1) packed in a globular arrangement very similar to what is seen for Ca^{2+}-bound GCAP1.[9] (D) Overlay of the main chain structure of GCAP5 (cyan) and the crystal structure of GCAP1 (red). The secondary structural elements are labeled as defined in Figure 1. The Ca^{2+} switch helix (α10) is colored purple. Cys15 and Cys17 side chain atoms are colored yellow. Bound Mg^{2+} is colored orange. The N-terminal myristoyl group is colored magenta. Side chain atoms of residues at the dimer interface (H18, Y21, M25, F72, and V76) and Mg^{2+} binding site (D63, D65, and D67) are indicated as sticks. (D) Overlay of main chain structures of Ca^{2+}-bound GCAP1 (red) and Ca^{2+}-free, Mg^{2+}-bound GCAP5 (cyan).

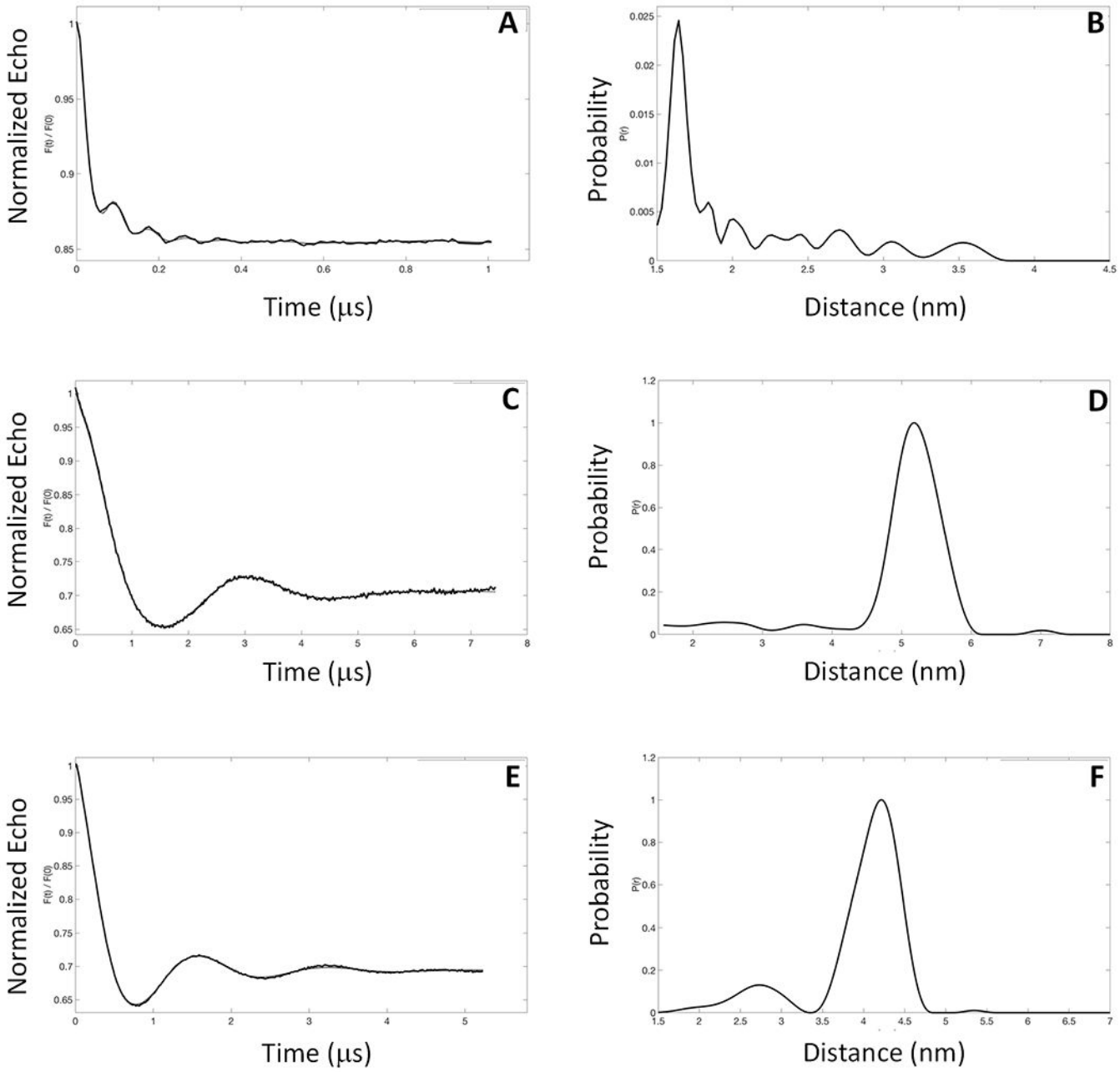

Figure 4.

EPR-DEER intermolecular distances for the GCAP5 dimer. Representative EPR-DEER data of (A) GCAP5^{CL}(A28C), (C) GCAP5^{CL}(N56C), and (E) GCAP5^{CL}(A69C) and corresponding distance distributions of (B) GCAP5^{CL}(A28C), (D) GCAP5^{cl}(N56C), and (F) GCAP5^{CL}(A69C). GCAP5 samples were in the Ca^{2+}-free, Mg^{2+}-bound state. Similar DEER data were observed for GCAP5 in the Ca^{2+}-bound state (not shown). A nitroxide spin-label (MTSSL) was covalently attached to the sole Cys residue in each mutant. The distance distributions and average intermolecular distances were calculated on the basis of the DEER data as described in Materials and Methods. The DEER intermolecular distances

were measured to be 16 ± 1 Å [GCAP5^{CL}(A28C) in panel B], 52 ± 3 Å [GCAP5^{CL}(N56C) in panel D], and 41 ± 3 Å [GCAP5^{CL}(A69C) in panel F].

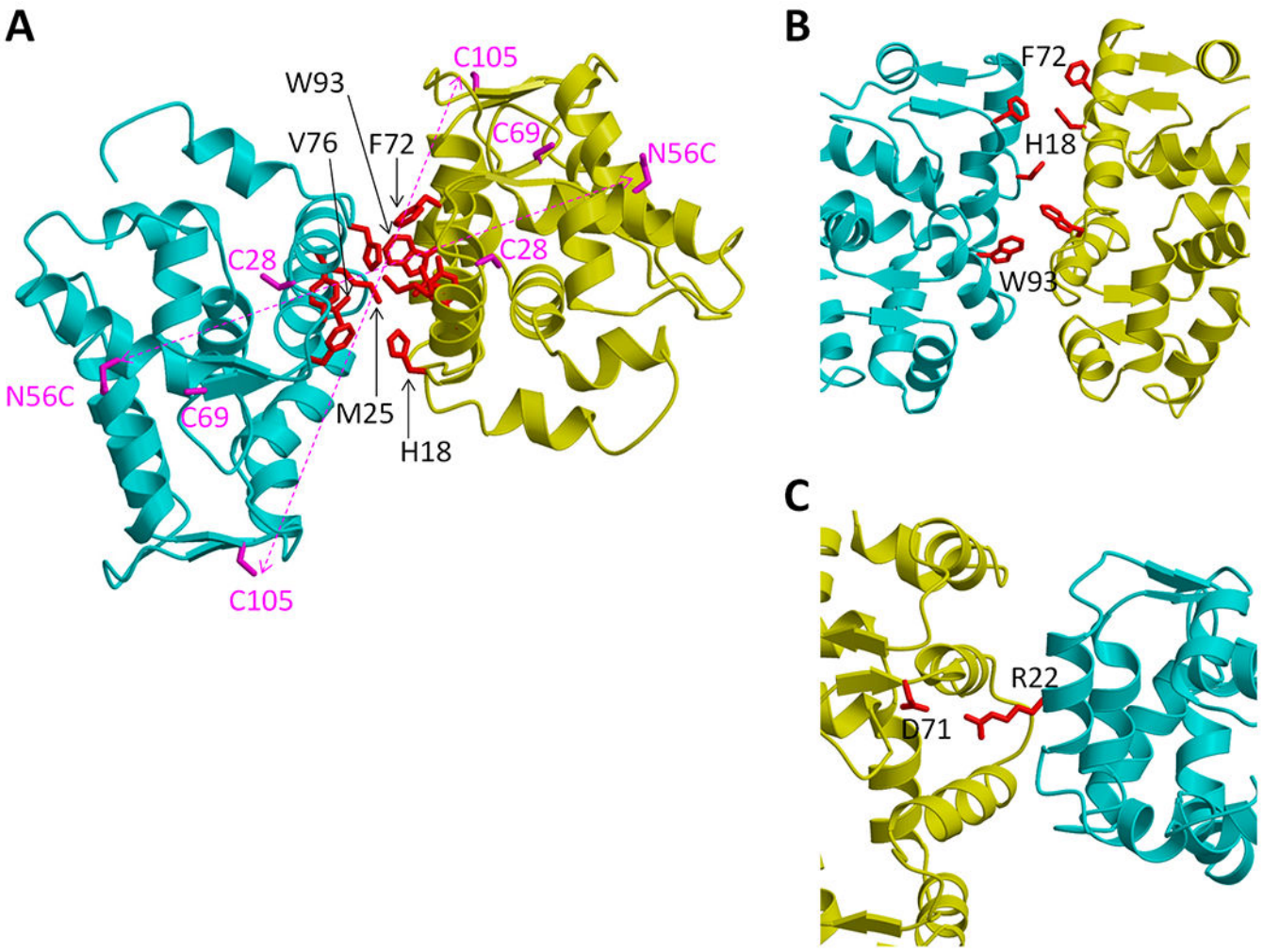

Figure 5.

Structural model of the GCAP5 dimer. (A) Ribbon diagram of the main chain structure of the GCAP5 dimer derived from DEER intermolecular distances listed in Table 2. The dimer subunits are colored cyan and yellow. Representative spin-labeled Cys residues for DEER studies (C28, N56C, C69, and C105) are colored magenta. Side chain atoms of residues at the dimer interface (H18, Y21, M25, F72, V76, and W93) are represented as sticks and are colored red. (B) Close-up of the dimer interface showing intermolecular contacts between aromatic residues. The side chain atoms of H18, F72, and W93 are colored red. (C) Close-up f the intermolecular salt bridge between R22 and D71.

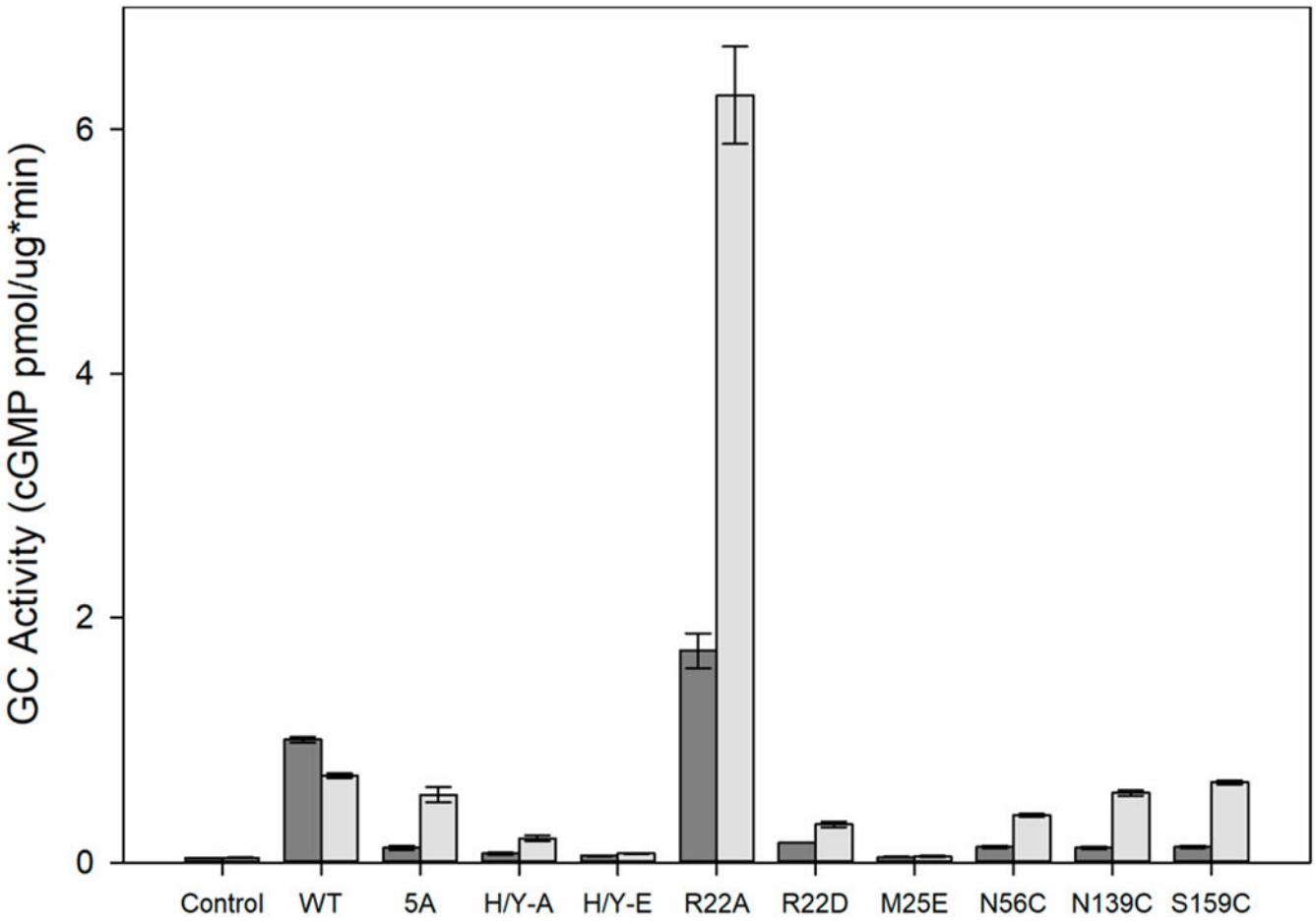

Figure 6.

Activation of photoreceptor guanylate cyclase by GCAP5 mutants. Purified myristoylated GCAP5 wild type (WT), Cys-less (5A), and variants (H18A/Y21A, H18E/Y21E, R22A, R22D, M25E, N56C, N139C, and S159C) were incubated with HEK293 cell membrane suspensions containing photoreceptor human guanylate cyclase (GC-E). The concentrations of wild type GCAP5 and variants were each 3 μM, and the free Ca^{2+} concentration was adjusted to 30 μM (dark gray bar) or 10 nM (light gray bar) using a Ca^{2+}/EGTA buffer system.

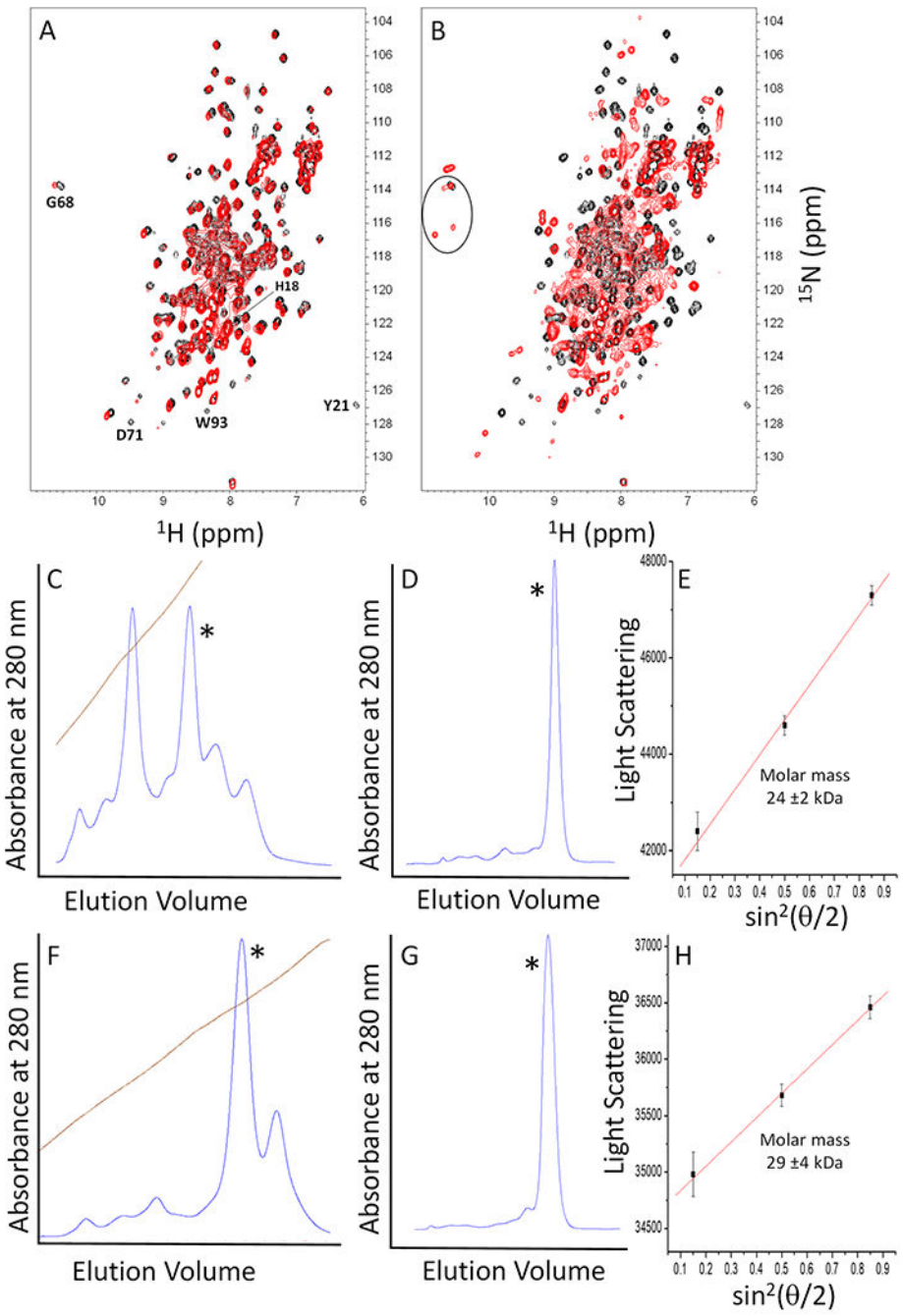

Figure 7.

NMR and SEC-MALS of GCAP5 dimerization site mutants. (A) ^{1}H–^{15}N HSQC spectra of ^{15}N-labeled GCAP5^{M25E} (red) and GCAP5^{WT} (black). (B) ^{1}H–^{15}N HSQC spectra of ^{15}N-labeled GCAP5$^{H18E/Y21E}$ (red) and GCAP5^{WT} (black). (C) Ion exchange chromatogram to isolate the monomeric fraction (marked by an asterisk) of GCAP5$^{H18E/Y21E}$. (D) Size exclusion chromatogram of GCAP5$^{H18E/Y21E}$. (E) MALS Zimm plot analysis of the monomeric fraction of GCAP5$^{H18E/Y21E}$ that determined a molar mass of 24 ± 2 kDa. (F) Ion exchange chromatogram to isolate a monomeric fraction (marked by an asterisk)

of GCAP5^{R22D}. (G) Size exclusion chromatogram of GCAP5^{R22D}. (H) MALS Zimm plot analysis of GCAP5^{R22D} that determined a molar mass of 29 ± 4 kDa. The experimental conditions for MALS are given in Materials and Methods.

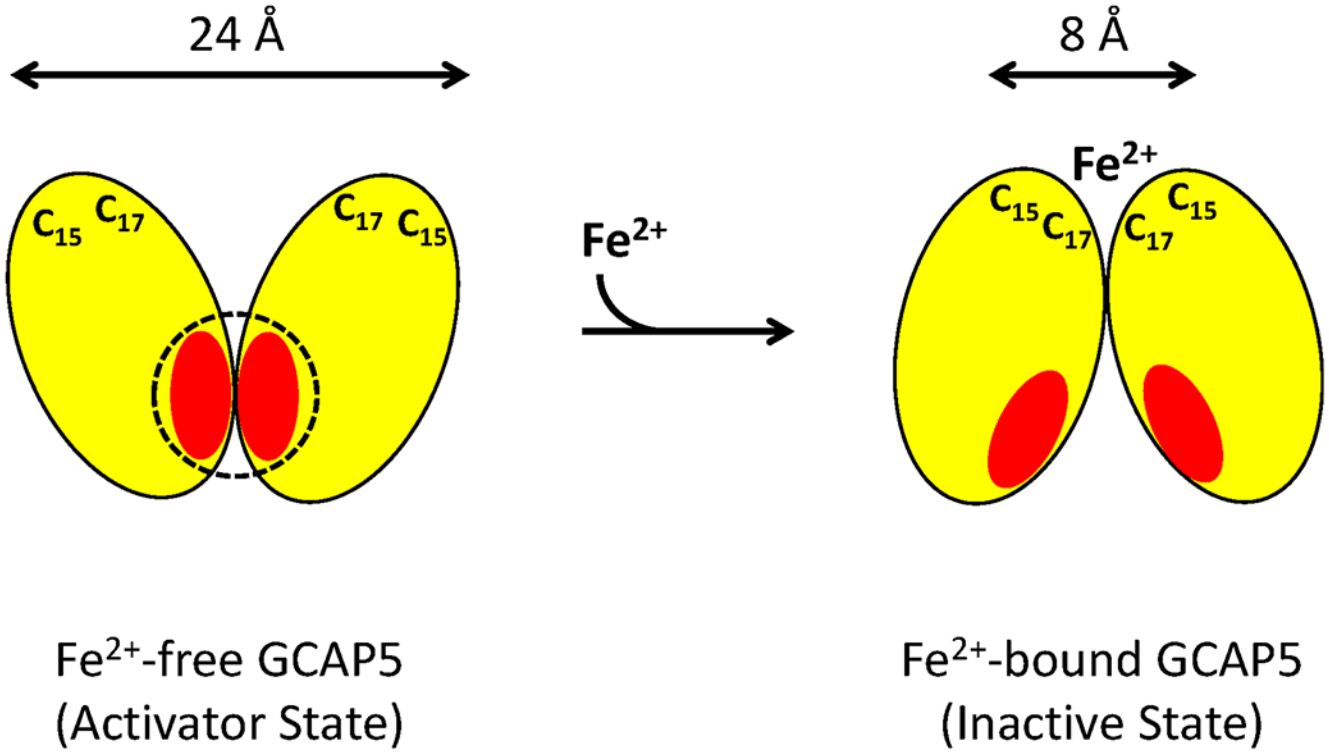

Figure 8.

Fe^{2+}-dependent structural changes in GCAP5. Schematic model of dimeric GCAP5 in the Fe^{2+}-free activator state (left) and Fe^{2+}-bound inactive state (right). A single bound Fe^{2+} is chelated by sulfhydryl side chains of Cys15 and Cys17 from both protein subunits of the GCAP5 dimer. The intermolecular distance between the Cys15 sulfhydryl group is depicted by a double arrow. GCAP5 residues (H18, Y21, M25, F73, V76, and W93) implicated previously in the binding to guanylate cyclase[54,55] are represented by red ovals, and the putative cyclase binding site is shown by a dotted circle.

Table 1.

NMR Structural Statistics for GCAP5

NMR restraints	**value (restraint violation)**
short-range NOEs	526 (0.0 ± 0.0)
long-range NOEs	145 (0.0 ± 0.0)
hydrogen bonds	144 (not used in water refinement)
dihedral angles	172 (0.1 ± 0.3)
$^{1}D_{HN}$ RDC	24 (0.0 ± 0.0)
RDC *Q*-factor	0.321
coordinate precision (Å)[a]	
RMSD for backbone atoms	1.0 ± 0.04
RMSD for all heavy atoms	1.6 ± 0.1
deviation from idealized geometry	
bonds (Å)	0.007 ± 0.001
angles (deg)	0.823 ± 0.015
impropers (deg)	0.925 ± 0.025
Ramachandran plot (%)	
favored region	78.1
allowed region	16.3
outlier region	5.6
structure quality[b]	
Clash score	80
Ramachandran outliers	5.6%
side chain outliers	6.1%

[a]Coordinate precision was calculated for residues 9–16, 20–41, 49–81, 89–120, 130–139, and 148–160.

[b]Structure quality metrics assessed by MolProbity.[36]

Table 2.

Molecular Docking Statistics for GCAP5

DEER distance restraint	C15 Sγ, 24 ± 6 Å
DEER distance restraint	C17 Sγ, 18 ± 2 Å
DEER distance restraint	T26C Sγ, 17 ± 2 Å
DEER distance restraint	C28 Sγ, 16 ± 1 Å
DEER distance restraint	N56C Sγ, 52 ± 3 Å
DEER distance restraint	C69 Sγ, 41 ± 3 Å
DEER distance restraint	C105 Sγ, 43 ± 11 Å
DEER distance restraint	N139C Sγ, 57 ± 4 Å
DEER distance restraint	E152C Sγ, 45 ± 4 Å
DEER distance restraint	S159C Sγ, 40 ± 3 Å
calculated distance	C15 Sγ, 32 Å
calculated distance	C17 Sγ, 28 Å
calculated distance	T26C Sγ, 16 Å
calculated distance	C28 Sγ, 21 Å
calculated distance	N56C Sγ, 52 Å
calculated distance	C69 Sγ, 39 Å
calculated distance	C105 Sγ, 52 Å
calculated distance	N139C Sγ, 57 Å
calculated distance	E152C Sγ, 42 Å
calculated distance	S159C Sγ, 42 Å
HADDOCK energy	−181.3 ± 5.8
RMSD (Å)[a]	0.9 ± 0.6
cluster size	11

[a]Root-mean-square deviation of backbone heavy atoms.